Roberts Massif 04261 and 04262

Enriched olivine-phryic shergottites
78.8 and 205 grams

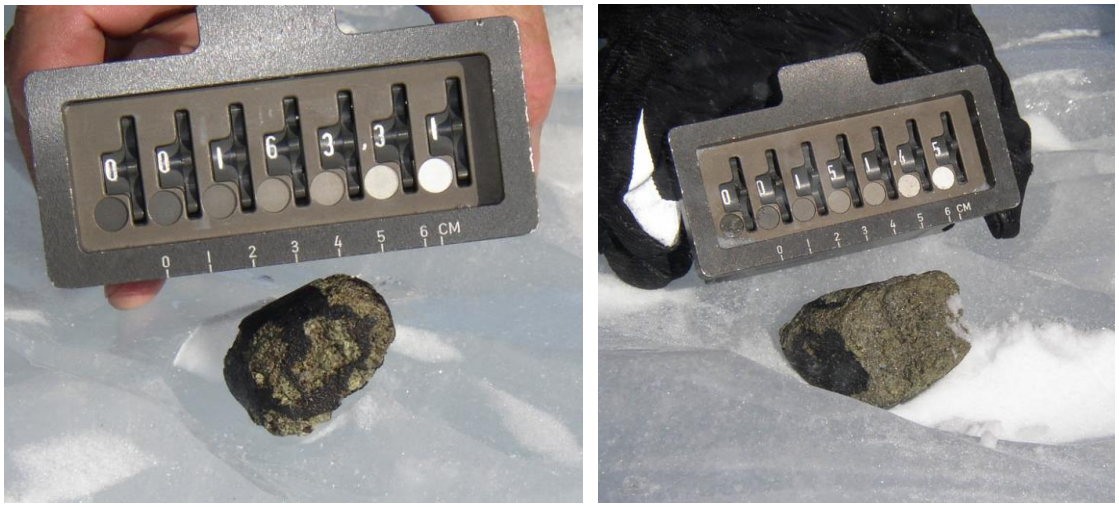

Figure 1: *Images of RBT 04261 and RBT 04262 found in the Roberts Massif dense collection area of the TransAntarctic Mtns during the 2004-2005 ANSMET season.*

Introduction

Two shergottites were found together on the ice (Figure 1) in the Roberts Massif in the TransAntarctic Mtns in 2004 (AMN vol. 30, no. 1; Feb. 2007). The Roberts Massif dense collection area is adjacent to the Grosvenor Mountains and near Larkman Nunatak (Figure 2). These two stones are partially fusion crusted and have a light grey interior with some indication of coarse and finer-grained lithologies (see also below).

Figure 2: *Location of Roberts massif adjacent to the Grosvenor Mtns and closest to Larkman Nunatak area.*

Figure 3: *RBT 04261 and RBT 04262 images taken in the NASA Johnson Antarctic Meteorite Laboratory*

Petrography

Brief descriptions of the petrography of RBT 04261 are found in AMN vol. 30, no. 1 and Connolly et al. (2007) and a complete description is found in Usui et al. (2010) (Table 1). About half of the exterior surfaces have a brown/black, rough-textured fusion crust. The interiors are soft and tan-grey in color with a sandy granular texture (Figure 3). Thin sections show a coarse-

grained assemblage of pyroxene, olivine and maskelynite (grain size about 4 mm; Figure 4). Shock-melt veins and pockets are present.

Anand et al. (2008), Dalton et al. (2008), Mikouchi et al. (2008), Mittlefehldt and Herrin (2008), Usui et al. (2008, 2010) and Shearer et al. (2009) have all reported on the petrology of RBT 04262. They find these rocks are made up of two distinct regions: a poikilitic region defined by large (5 mm) low-Ca pyroxene oikocrysts including small olivine chadocrysts, chromites and melt inclusions and a non-poikilitic region with intergrown maskelynite, olivine, pyroxene, phosphates, chromite, ilmenite and sulfides. Anand et al. consider RBT 04262 to be an olivine cumulate and, indeed, *"ghosts"* have been reported in P scans of olivine (Beckett et al. 2008). Papike et al. (2009) have compared these various shergottites, and confirmed the earlier mineral chemistry.

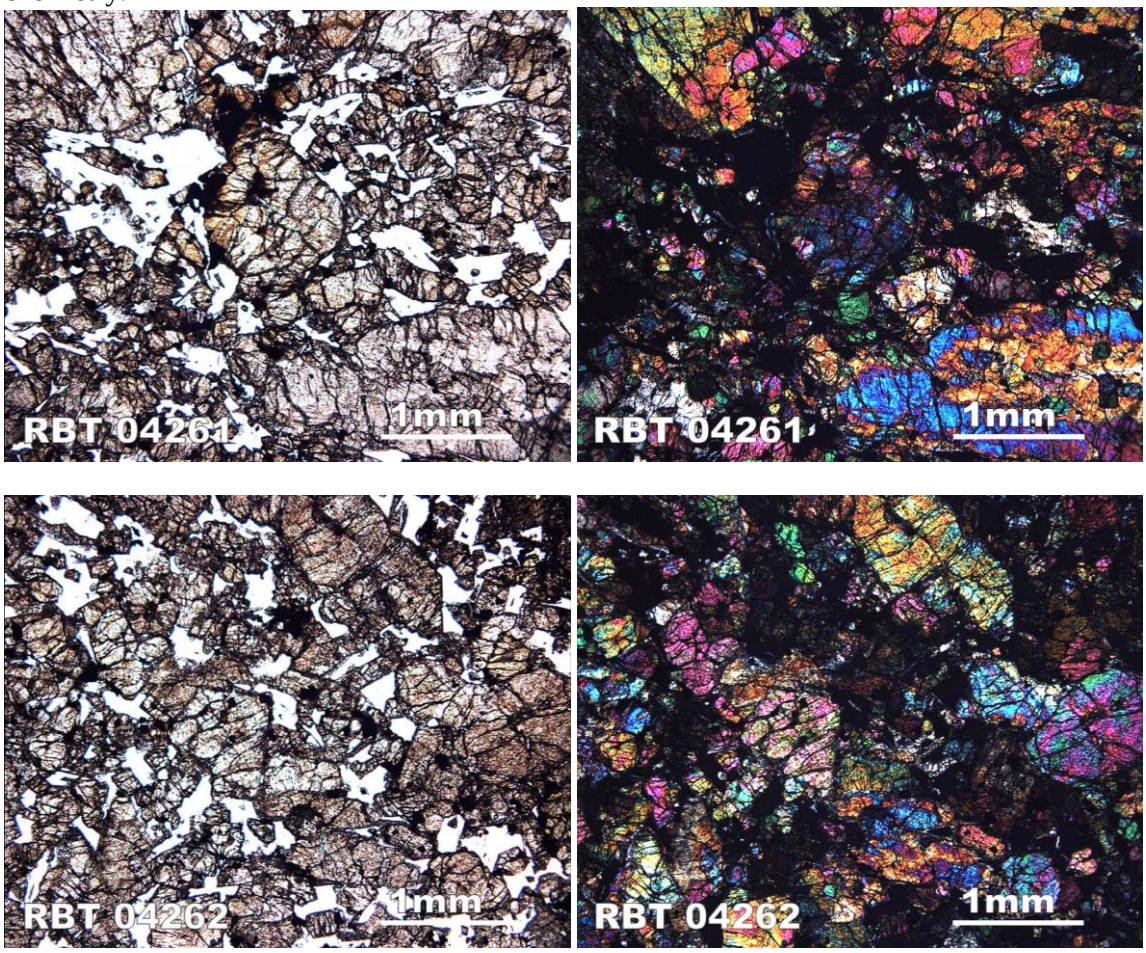

Figure 4: *transmitted and cross polarized light images of the RBT 04261 and RBT 04262 shergottites.*

Several investigators have established that RBT 04261 and 04262 consist of poikilitic and non-poikilitic lithologies (Figure 5; e.g., Anand et al., 2008; Mikouchi et al., 2008; Usui et al., 2010). The non-poikilitic area comprises ~80% and the poikilitic ~20% of the total (Usui et al., 2010). There may also be a reaction zone between the two which Shearer et al. (2008) called "lithology C". The poikilitic lithology is composed of pyroxene oikocrysts (low-Ca pyroxene with up to ~1 mm high-Ca pyroxene rims) with chromite and small (0.5 mm) rounded olivine chadacrysts within. The non-poikilitic lithology is

Table 1: Mineralogical Mode for RBT 04262

	Mikouchi 2008	Usui et al. 2010	
		261	262
Olivine	30 %	42.1	39.4
Pyroxene			
Pigeonite	43	21.5	28
Augite	10	10.7	12.4
Plagioclase	13	20.2	15.9
Chromite	2	1.6	1.5
Ilmenite		0.2	0.2
Phosphate	1	1.8	1.1
Other	1	1.9	1.4

interpreted to have formed from an intercumulus melt that was more evolved than the parental melt of the poikilitic lithology and was probably co-saturated with olivine, high and low-Ca pyroxenes, and plagioclase (Usui et al., 2010). Mikouchi et al. (2008) found RBT 04262 to be composed of subequal amounts of the poikilitic and non-poikilitic areas, and determined modal mineralogy (Table 1). Plagioclase occurs only in the non-poikilitic areas. The abundance of olivine chadacrysts is much smaller than that in typical lherzolitic shergottites.

Kaersutite-bearing magmatic inclusions are found in the pyroxene oikocrysts (Park et al., 2013; Mikouchi et al., 2008). Anand et al. (2008) also noted partially re-crystallized melt-inclusions rich in late-stage fractionates such as K-rich feldspathic glass, phosphates and opaque oxides inside olivine and pyroxene grains.

Shock metamorphism is intensive, but shock melt appears to be rare. A small shock melt pocket ~500 μm in size was observed by Mikouchi et al., 2008 and Park et al. (2013), and a thin melt vein was characterized by Takenouchi et al. (2018) (see below).

Mineralogy

Olivine: Usui et al. (2010) noted that the poikilitic areas had olivine that was "distinctly higher in forsterite content" (Fo_{60-70}) than the olivine in the non-poikilitic areas (Fo_{57-62}). Beckett et al. (2008) illustrated rather strange phosphorous zoning in olivine from RBT.

Pyroxene: Low-calcium pyroxene oikocrysts are abundant (Mikouchi et al. 2008; Anand et al. 2008; Usui et al. 2010). They are rimmed by high-calcium pyroxene approaching augite in composition (Figure 6a,b).

Plagioclase: The plagioclase in RBT shergottites has been converted to maskelynite by shock. It has a range of composition from An_{56} to An_{22} and is more sodic than is found in the other olivine-phyric shergottites (Usui et al., 2010). Some maskelynite in RBT is also potassic ($An_{15}Ab_{64}Or_{21}$).

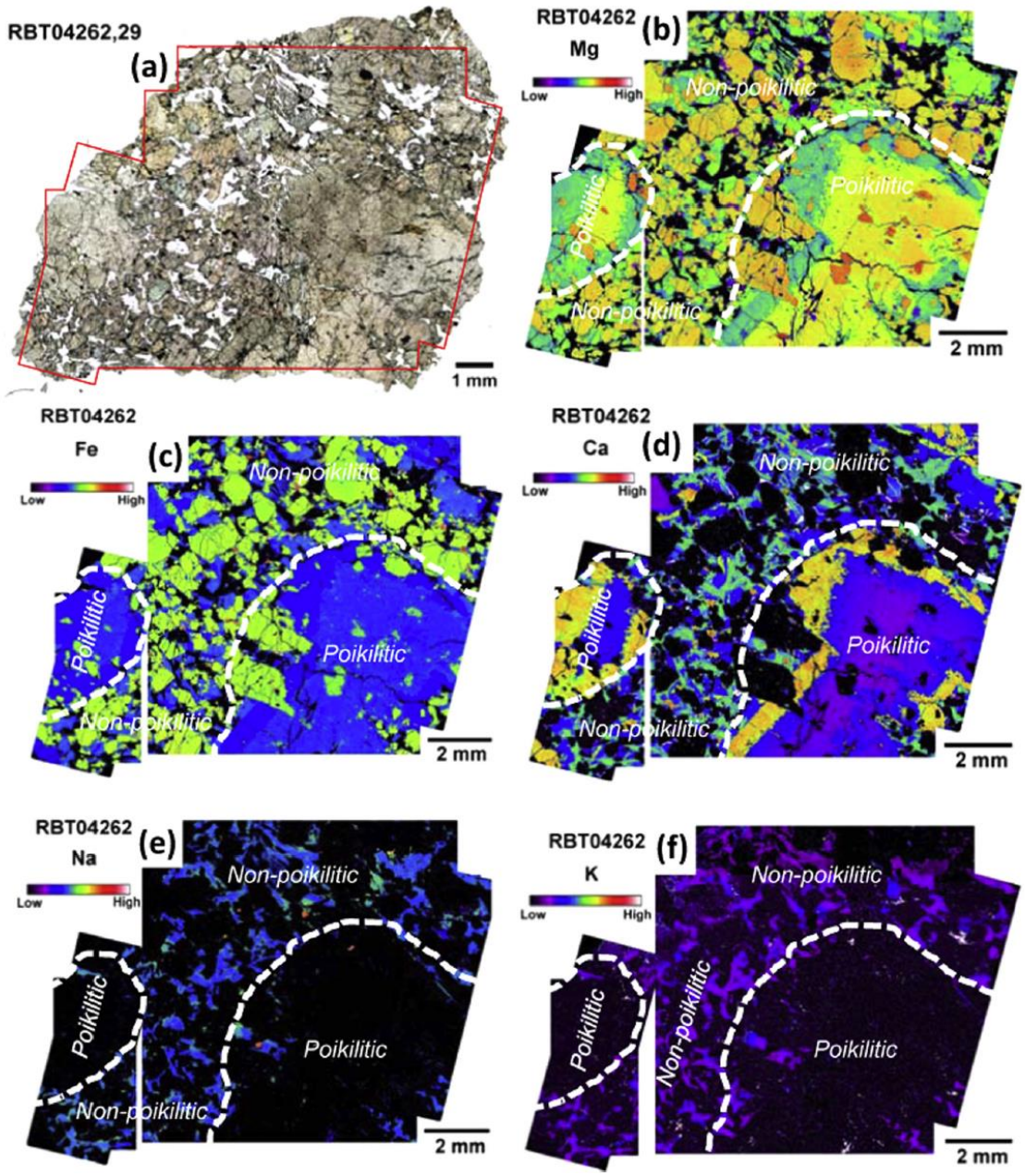

Figure 5: *Textural and compositional features of the poikilitic and non-poikilitic lithologies of RBT 04261 and 04262 (from Park et al., 2013).*

Opaques: Al-rich chromites have two distinct trends in RBT shergottites (see Usui et al. 2010). The chromites in the mafic poikilitic regions vary from Chr_{52} to Chr_{77}, while the chromites in the non-poikilitic regions vary from Ulv_{2} to Ulv_{37}.

Phosphate: The phosphate in RBT 04262 is merrillite (Figures 7 and 13: Usui et al., 2010; Shearer et al., 2014), which contains most of the meteorite's REE budget.

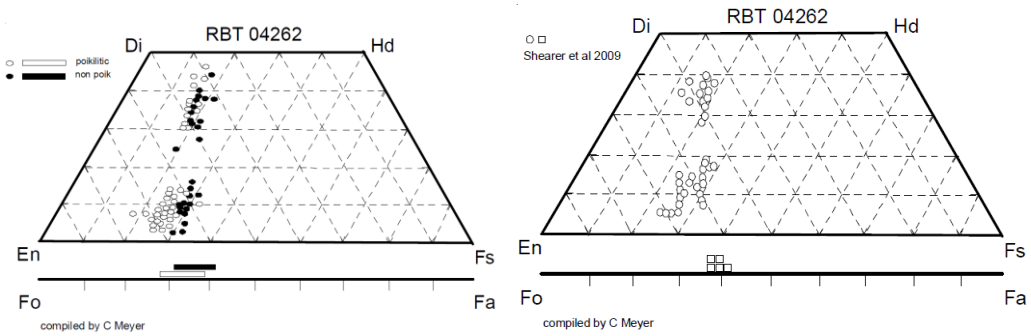

Figure 6: *Olivine and pyroxene compositions from RBT 04262 from Mikouchi et al., 2008) (left) and Shearer et al. (2009) (right).*

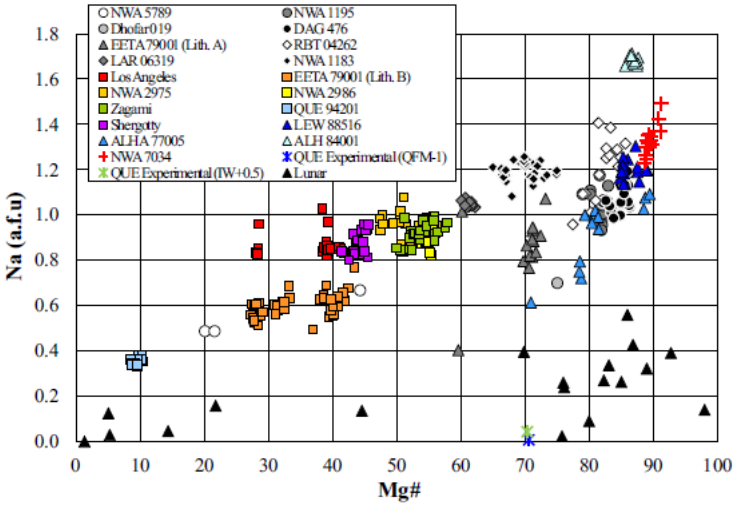

Figure 7: *Range of merrillite compositions in suite of Martian meteorites described by Shearer et al. (2014). Note Na-rich nature of Martian merrillites compared to lunar samples.*

Shock melt veins: RBT 04261 contains a thin shock vein ~60 μm in width which looks black under plane polarized light. The vein mainly consists of mineral fragments and fine-grained matrices, and their compositions are influenced by the surrounding minerals. The matrices mainly consist of glassy material because Raman analyses of the matrices show only broad peaks, but the main peaks of ringwoodite were also observed (800 and 840 cm^{-1}) and the EBSD pattern is similar to a simulated ringwoodite pattern (Figure 8; Takenouchi et al., 2018). Olivine around the shock vein is darkened, shows lamellar structure, looks brighter than the other areas in BSE, and its EBSD patterns are ambiguous, suggesting a disordered crystal structure. In addition, a small increase in Fe^{3+} is detected by XANES analysis (Takenouchi et al., 2018).

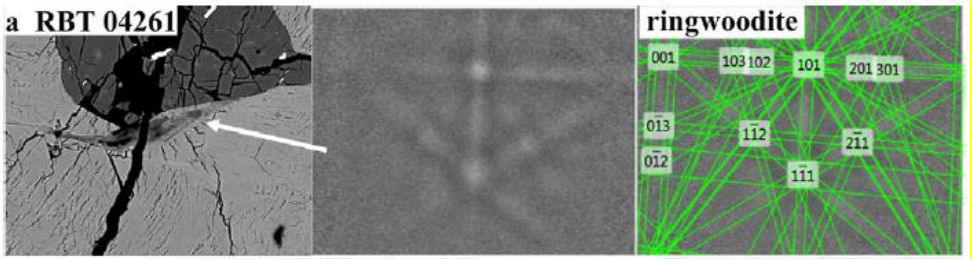

Figure 8: *Kikuchi and EBSD pattern indicating ringwoodite in RBT 04261 melt pocket (from Takenouchi et al. (2018).*

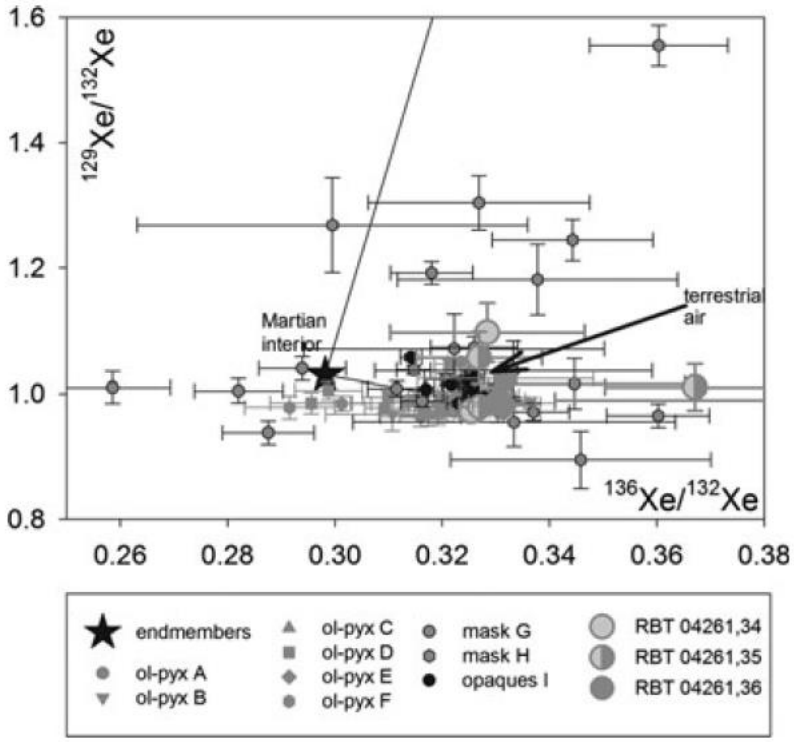

Figure 9: *Xe isotopes in RBT 04261 measured by Schwenzer et al. (2013) along with data from Cartwright et al. (2010).*

Weathering

Xenon isotopes and halogen contents have been reported by Cartwright et al. (2008, 2009). Cartwright et al. (2010) reported an exhaustive study of all the minerals in RBT and other shergottites, and found that while some minerals contain excess ^{129}Xe, other minerals contain excess ^{40}Ar, suggesting different sources.

Schwenzer et al. (2013 measured noble gases and oxygen with an interest in assessing their influence by alteration. For the most part, He, Ne, Ar, and O isotopes are not strongly affected by weathering. The heavy noble gases are most seriously affected by alteration, in some subsamples to the extent that no Martian signatures can be detected anymore. Their results demonstrated that a visibly clean interior portion of a meteorite is not necessarily free from terrestrial contamination in the heavy noble gases. RBT 04261, which is essentially free from any visible alteration at electron microprobe investigation scale, is contaminated by fractionated terrestrial noble gases (EFA) throughout, with the most serious effects on Xe (Figure 9). Even in stepwise heating experiments (see data of Cartwright et al., 2010 in Figure 9), the amount and degassing behavior of this contamination seriously compromise the interpretation of the Martian signature in the meteorite.

Greenwood et al. (2009) examined hydrogen isotopes in jarosite and gypsum in RBT 04262 and found a light isotopic composition in the jarosite that suggests formation in Antarctica, whereas heavier hydrogen in gypsum may have formed in Houston (or Mars or Antarctica).

Petrology

Oxygen fugacity

Usui et al. (2010) estimated equilibration temperature (T) and oxygen fugacity (fO_2) using 2-pyroxene thermometry, olivine–spinel geothermometry, olivine–orthopyroxene–spinel oxygen barometry, and Eu oxybarometry. Assuming that RBT 04261/04262 crystallized at near surface 1 bar conditions two-pyroxene geothermometry yields an equilibration temperature for a pigeonite and augite pair of ~1150 °C, whereas coexisting olivine–spinel–orthopyroxene grains yield an equilibration temperature of 827 ± 50 °C, and QFM-1.59±0.05. D_{Eu}/D_{Gd} values of 0.45±0.12 and 0.41±0.12 calculated for RBT 04261 and RBT 04262, respectively, translate to fO_2 estimates of QFM-2.2 and QFM-2, respectively. Examining the Fe^{3+}/Fe^{2+} ratio in maskelynite, Satake et al. (2014) found RBT 04262 has the highest Fe^{3+}/Fe^{2+} ratio of any shergottite (80% Fe^{3+}; Figure 10) - higher than depleted / intermediate shergottites, and highest among many other enriched shergottites (Figure 11). All these fO_2 estimates are relatively high for shergottites and indicate the RBT shergottites likely crystallized from a more oxidized environment.

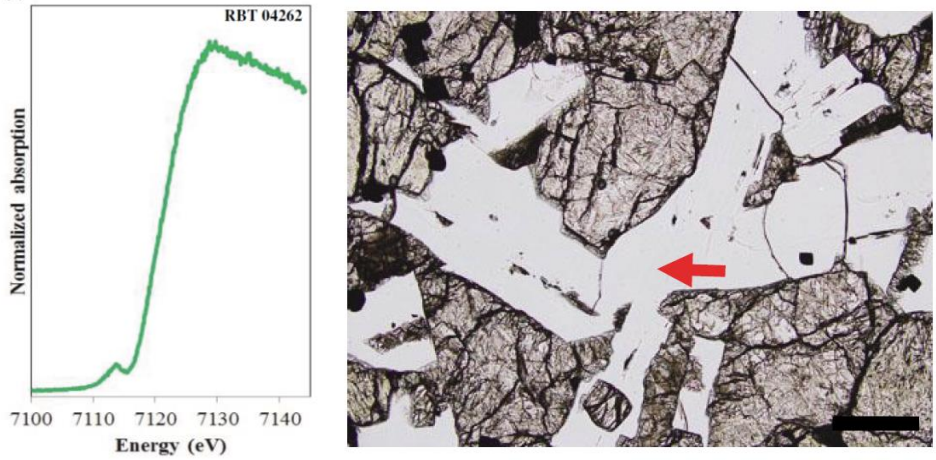

Figure 10: *XANES spectrum from maskelynite from RBT 04262 (from Satake et al., 2014).*

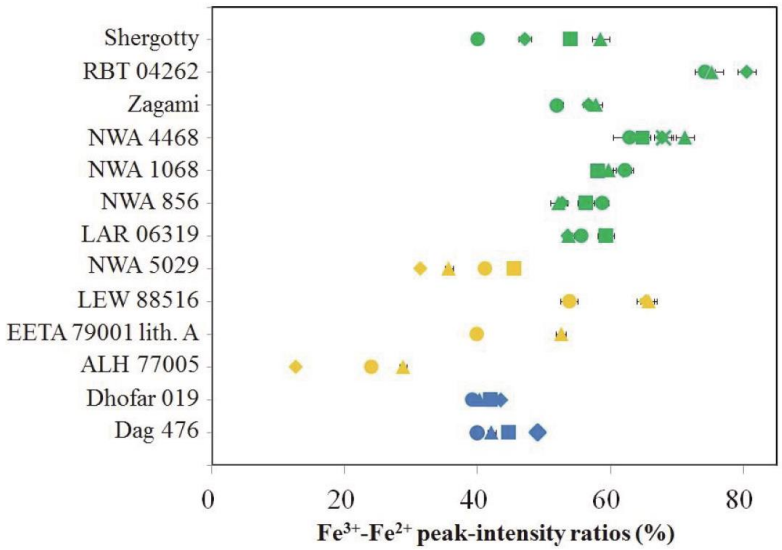

Figure 11: *Summary of XANES measurements on shergottite maskelynite showing oxidized nature of RBT 04262 compared to all others. (from Satake et al., 2014).*

Volatiles

Apatites in RBT 04261 and RBT 04262 have been analyzed for F, Cl, and OH to assess the volatile history recorded by this mineral. The high F and Cl have been used to argue that RBT crystallized from a F and Cl dominated magma, and that H_2O degassing and crystal fractionation played a small role in establishing the apatite compositions (Filiberto et al., 2016; McCubbin et al., 2016). On the other hand, Bellucci et al. (2017) argue that the high halogen contents of the RBT apatites indicate an important role for a halogen-rich fluid with negative $\delta^{37}Cl$ values (Figure 12; see also stable isotope section below).

Chemistry

The chemical composition of RBT 04262 has been reported by Anand et al. (2008) (Table 2). The REE pattern is essentially flat, like that of Shergotty, but slightly lower (Figure 13). The enrichment of LREE relative to the depleted shergottites is the reason this sample is classified as an enriched shergottite. Walker et al. (2009), Brandon et al. (2012), and Tait and Day (2018) reported data on the highly siderophile element contents. Wang and Becker (2017a,b) report data for Cu and Ag in LAR 06319.

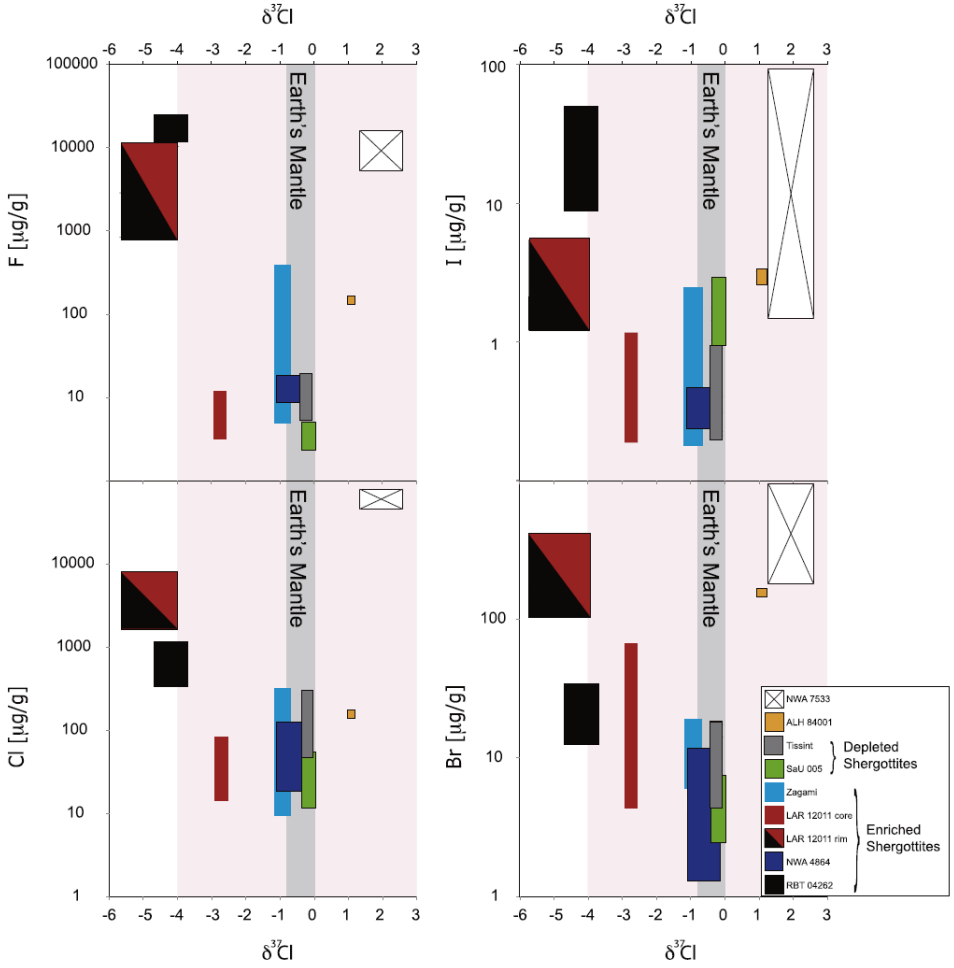

Figure 12: *correlations between halogen contents and chlorine isotopes measured by Bellucci et al. (2017).*

Table 2: Bulk composition of RBT 04262

reference	Anand 2008	
weight		
SiO_2 %	47.6	(a)
TiO_2	0.43	(a)
Al_2O_3	3.32	(a)
FeO	20.6	(a)
MnO	0.53	(a)
MgO	21.6	(a)
CaO	5.66	(a)
Na_2O	0.59	(a)
K_2O	0.08	(a)
P_2O_5	0.39	(a)
S %	0.17	(b)
sum		
Sc ppm	31	(b)
V	218	(b)
Cr	7152	(b)
Co	63	(b)
Ni	291	(b)
Cu	6.6	(b)
Zn	74	(b)
Ga	8.2	(b)
Ge ppb		
As		
Se		
Rb	4	(b)
Sr	22.2	(b)
Y	9.3	(b)
Zr	23	(b)
Nb		
Mo	0.4	(b)
Ru		
Rh		
Pd ppb		
Ag ppb		
Cd ppb	42	(b)
In ppb		
Sn ppb	110	(b)
Sb ppb	83	(b)
Te ppb		
Cs ppm	0.29	(b)
Ba	12.8	(b)
La	1.15	(b)
Ce	2.81	(b)
Pr	0.414	(b)
Nd	2.07	(b)
Sm	0.81	(b)
Eu	0.314	(b)

Gd	1.36	(b)
Tb	0.26	(b)
Dy	1.75	(b)
Ho	0.4	(b)
Er	1.07	(b)
Tm	0.155	(b)
Yb	0.96	(b)
Lu	0.145	(b)
Hf	0.97	(b)
Ta		
W ppb	380	(b)
Re ppb		
Os ppb		
Ir ppb		
Pt ppb		
Au ppb		
Th ppm	0.257	(b)
U ppm	0.058	(b)

technique: (a) ICP-AES, (b) ICP-MS

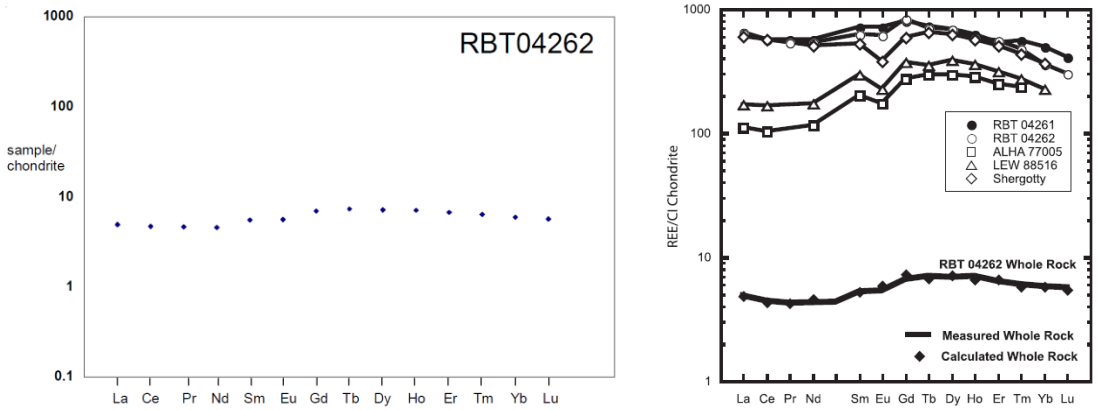

Figure 13: *Rare Earth element concentrations (chondrite normalized) for RBT 04261 and RBT 04262 measured in whole rocks by Anand et al. (2008) (left) and Usui et al. (2010) (right). The right diagram also shows merrillite REE data for RBT and several other shergottites.*

Radiogenic age dating

RBT 04262 was dated by the Lu-Hf technique with an age of 225 ± 21 Ma (Lapen et al. 2008)(Figure 14). However, Shih et al. (2009) reported significantly younger ages (174 ± 14 Ma by Sm-Nd and 167 ± 6 Ma by Rb/Sr) (Figures 15 and 16; Table 3).

The RBT shergottites became involved in the debate about the age of shergottites. Some analysis suggested shergottites record a 4.1 Ga ages, but may have been reset by younger shock events (Bouvier et al., 2010). This prompted Niihara to date small (<5 micron) baddeleyite grains in RBT – baddeleyite is thought to be robust to shock and thus should record the age of crystallization (Figure 17). Niihara (2011) demonstrated that RBT 04262 baddelyites define an age of ~ 200 Ma (Figure 18).

Examining the same issue, but with Lu-Hf and Sm-Nd, Bloch and Ganguly (2014) measured diffusion of Hf in diopside and concluded that the timescale required for shock resetting of RBT 04262 is much longer than the time available in post-shock heating. They also suggest the 200 Ma Lu-Hf age measured by Lapen et al. (2008) is a crystallization age.

Table 3
Summary of Age Data for RBT 04262 (Ma)

	Lu-Hf	Sm-Nd	Rb-Sr
Lapen et al. 2008	225(±21)		
Shih et al. 2009		174(±14)	
			167(±6)

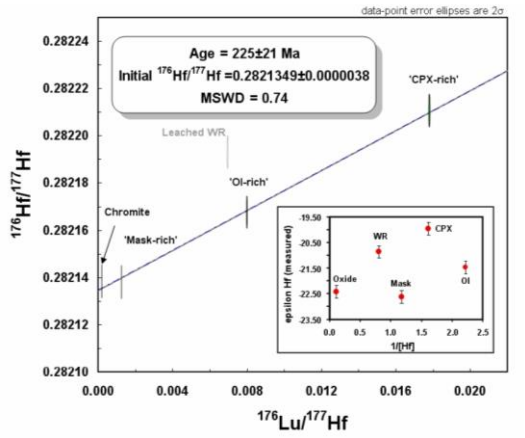

Figure 14: *Lu-Hf isochron for RBT 04262 from (Lapen et al., 2008).*

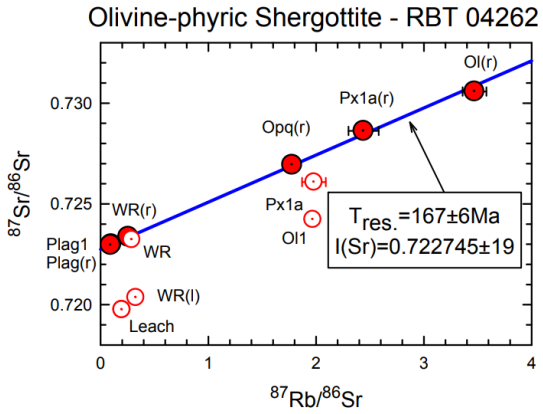

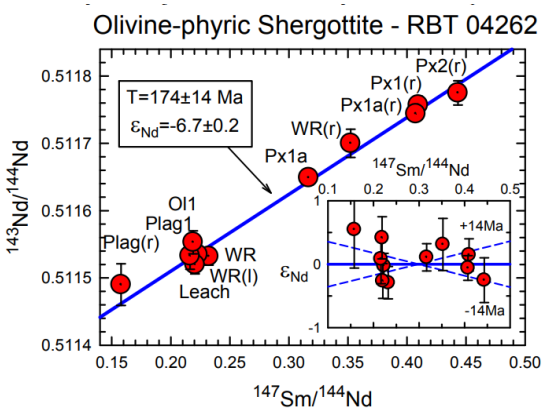

Figure 15: *Rb-Sr isochron for RBT 04262 reported by Shih et al. (2009).*
Figure 16: *Sm-Nd isochron for RBT 04262 reported by Shih et al. (2009).*

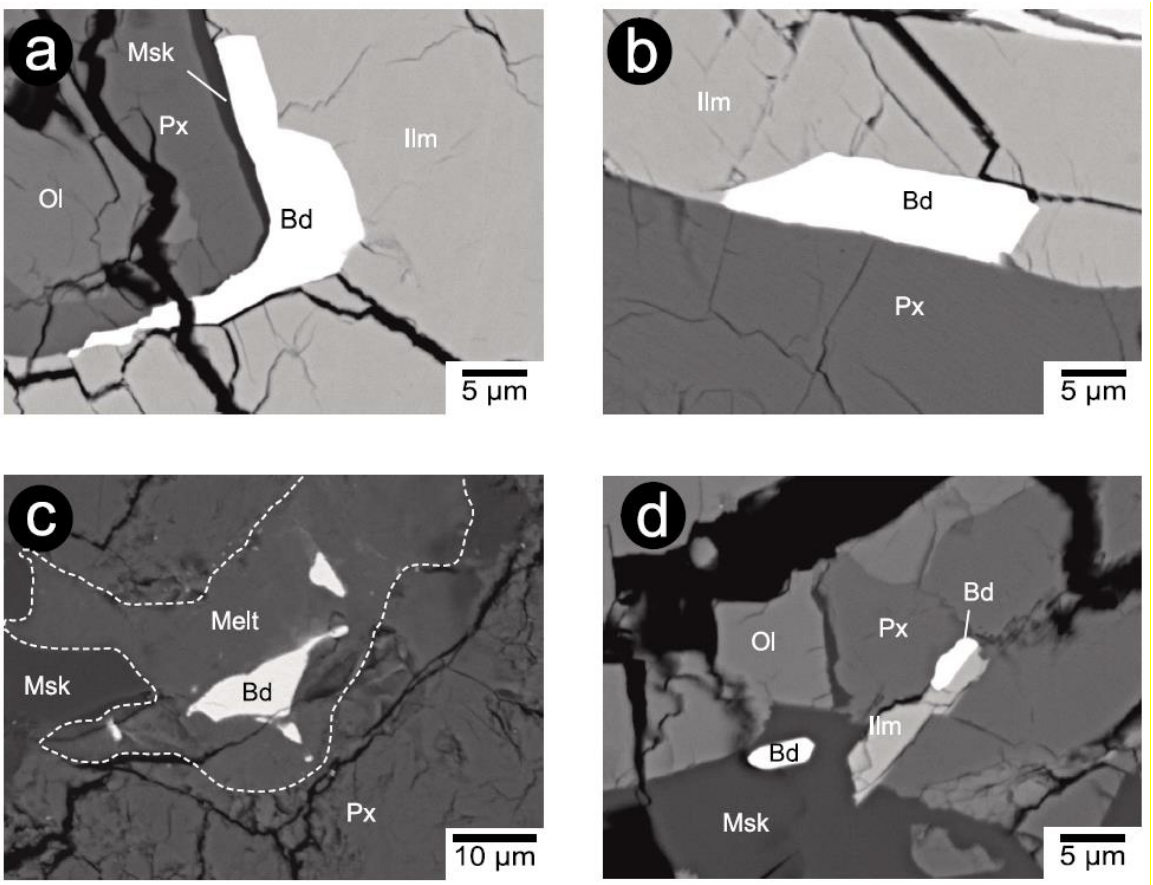

Figure 17: *Baddeleyite grains analyzed for U-Pb dating using SIMS reported by Niihara (2011).*

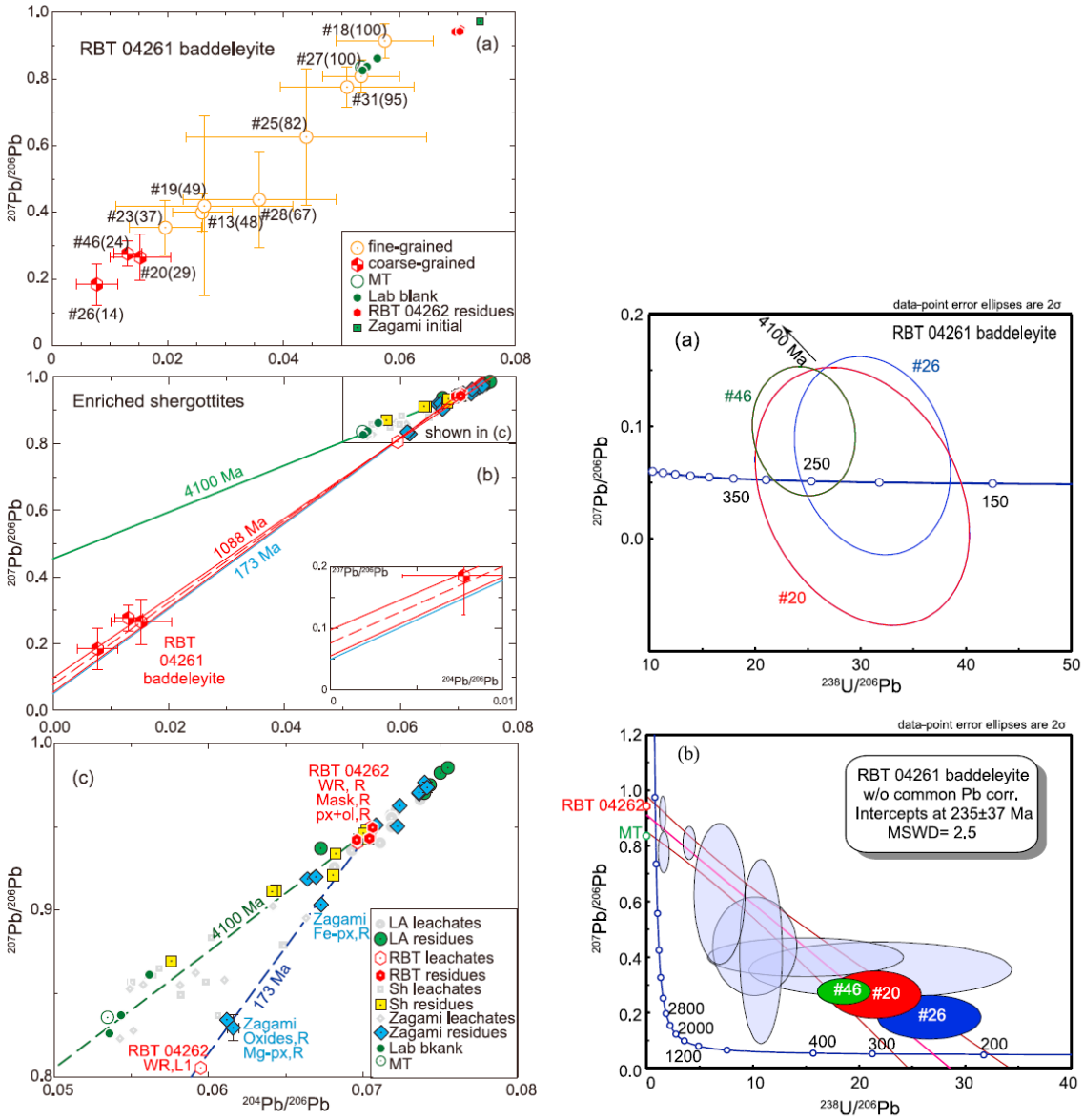

Figure 18: *Pb-Pb and U-Pb systematics of RBT 04261 and RBT 04262 measured by Niihara (2011), as well as data from other shergottites (Los Angeles, Shergotty, Zagami).*

Park et al. (2013) reported Ar-Ar measurements for RBT 04262, and showed that the Ar in RBT and many other shergottites is affected by trapped components that influence the interpretation of ages. For RBT 04262 maskelynite, the 850–1050 °C extractions (22–78% ^{39}Ar) yielded an isochron age of 171 ± 8 Ma, in excellent agreement with the well-behaved Sm–Nd isochron of 174 ± 14 Ma (Shih et al., 2009). Some older ages also have been reported for RBT 04262 as well. Lapen et al. (2008) reported a Lu–Hf age of 225 ± 21 Ma, for example. Ages somewhat older than 171 ± 8 Ma can be obtained by selecting different portions of the Ar release, but all selections for intermediate temperature extractions (750–1050 °C) yielded ages in the range 171–206 Ma for initial ^{40}Ar/^{36}Ar in the range 420–680 (Table 5). Ages derivable from the RBT-WR and RBT-Px data are

based on low-temperature (300–600 °C) data for which the isochron intercepts and ages are dominated by air Ar, and are considered less reliable.

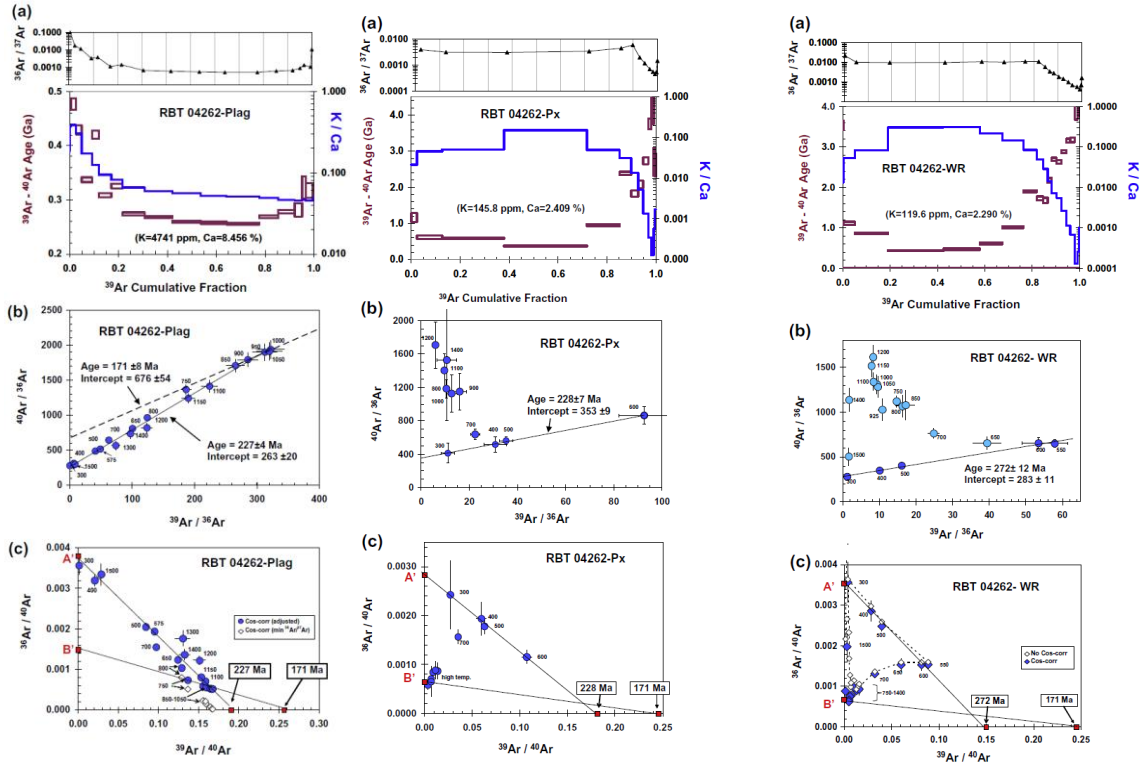

Figure 19: *Ar-Ar systematics of the RBT 04262 plagioclase, clinopyroxene, and whole rock, reported by Park et al. (2013).*

The poikilitic/non-poikilitic texture of RBT and the presence of large pyroxene oikocrysts allowed a clear definition of Trapped-B, which is most likely the Martian atmosphere incorporated into RBT by assimilation of crustal rocks. Trapped-A represents terrestrial air. Trapped-A mixed in different proportions with Trapped-B could give apparently intermediate trapped $^{40}Ar/^{36}Ar$ compositions commonly observed in shergottites (Park et al., 2013).

Cosmic ray induced radiochemistry

Nishiizumi and Caffee (2010) reported a ^{10}Be exposure age of 3.0 ± 0.6 Ma for RBT 04261 and 2.0 ± 0.5 Ma for RBT 04262. They calculate a terrestrial age of 710 ± 60 Ka from ^{36}Cl. Nagao and Park (2008) reported an average cosmic ray exposure age of 2.3 ± 0.6 Ma from rare gas measurements.

Other Studies

Oxygen isotopes are reported by McBride et al. (2007) and Anand et al. (2008). Schwenzer et al. (2013) show that terrestrial weathering in Antarctica had little or no effect on the oxygen isotopic compositions, perhaps due to the short terrestrial age or residence time in the ice (<60 Ka for RBT 04261 and ~710 Ka for RBT 04262; Nishiizumi and Caffee, 2010).

Many stable isotope studies are aimed at deciphering the building blocks of Mars, such as Li, Ca, Mg, and Fe isotopes:
Li - RBT 04262 was used, along with a suite of Martian meteorites, to estimate the Li isotopic composition of the Martian mantle. This work by Magna estimated the δ^7Li for Mars to be 4.2 +/- 0.9, within error of the estimate for Earth's mantle 3.5 +/- 1.0 (Magna et al., 2015a).
Ca - Magna et al. (2015b) measured Ca isotopes in a suite of Martian meteorites, including RBT 04262, and found that Mars has identical Ca isotopic composition to Earth and Moon. They suggest the inner solar system is homogeneous with respect to Ca isotopic composition.
Mg - Magna et al. (2017) examined Mg isotopic composition of a suite of Martian meteorites and made a similar finding to that for Li and Ca – that Mars silicate mantle has a δ^{26}Mg value that is identical to that for the rest of the inner solar system.
Fe - Sossi et al. (2016) measured Fe isotopes in a suite of Martian meteorites (including RBT 04262) and found that when all are corrected for magmatic fractionation, the Martian mantle has δ^{57}Fe slightly lighter than Earth, but identical to chondrites and HEDs.

Williams et al. (2016) and Sharp et al. (2016) measured Cl isotopes in Martian meteorites and proposed that the lightest values of δ^{37}Cl (~ -4) represent the mantle and that heavier values up to ~ +1, represent interaction with crust or surface lithologies. This interpretation is at odds with that of Bellucci et al. (2017) who measured Cl isotopes and halogens in phosphates from Martian meteorites (Figure 12). They conclude that phosphates with no textural, major element, or halogen enrichment evidence for mixing with this surface reservoir have an average δ^{37}Cl of −0.6‰, which supports a similar initial Cl isotope composition for Mars, the Earth, and the Moon. Oxidation and reduction of chlorine are the only processes known to strongly fractionate Cl isotopes (both (+)ve and (-)ve), and perchlorate has been detected on the Martian surface, which has 5000 ppm Cl. Perchlorate formation and halogen cycling via brines has been active throughout Martian history, and has a significant influence of the Cl isotopic composition (Bellucci et al., 2017).

Franz et al. (2008, 2014) measured S isotopes in a large set of Martian meteorites including RBT 04261. They found it contains 1100 ppm total S, which was 800 ppm Acid Volatile Sulfide and 300 ppm sulfate. Among most samples in their study, the variability in Δ^{33}S is similar to that in chondritic sulphur and terrestrial mantle Sulphur - <0.01%, implying that sulphur was well mixed in the most abundant inner Solar System materials. The δ^{34}S values derived from shergottites AVS data from their study are also homogeneous and yielded a mean value within error of the standard (CDT) value, suggesting efficient mixing in the Martian mantle and little or no fractionation of sulphur isotopes during core formation. They found significant deviations from the mean in only three shergottites, which they ascribe to photochemical Martian atmospheric effects, and mid-crustal and near surface assimilation in some of the basaltic shergottites.

Differentiation

Constraints on the differentiation of Mars come from Pb and W isotopes. Bellucci et al. (2018) showed that there are two distinct Pb isotopic reservoirs using Martian meteorites, including RBT 04262. One reservoirs has a μ_1 value near 1.8, while the other has a μ_2 value from 2 to 4 (Figure 20). Kruijer et al. (2017) measured W isotopes on a suite of Martian meteorites, to help constrain the timing of mantle differentiation for Mars. RBT 04262 and other shergottites define an array in $\varepsilon^{182}W$ and La/Sm or $\varepsilon^{182}W$ and $\varepsilon^{143}Nd$ space indicating that Mars differentiated within 25-40 Ma after T_0 (Figure 21).

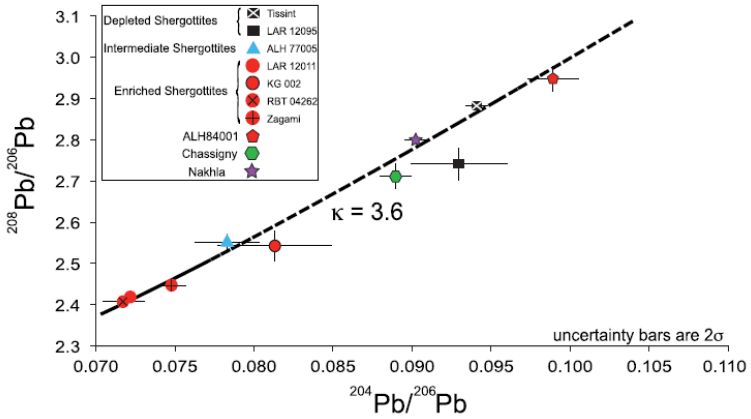

Figure 20: *Pb-Pb isotopic data indicating the presence of a Martian mantle reservoir with a distinct μ_2 value near 3.6 (from Bellucci et al., 2018).*

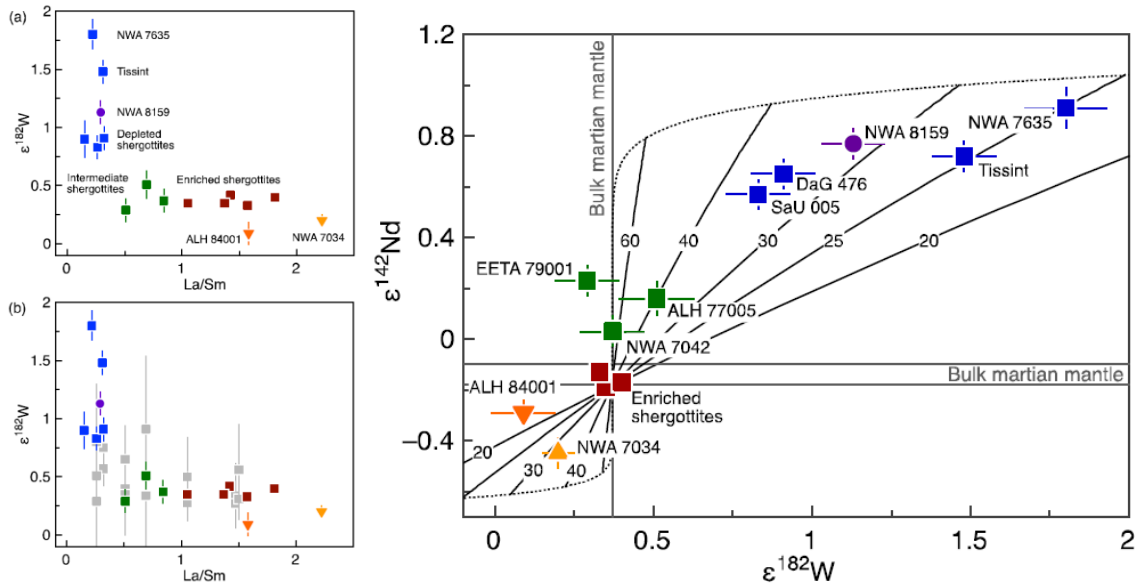

Figure 21: *Tungsten and Nd isotopic data for shergottites showing that the mantle must have differentiation between 25 and 40 Ma after T_0 (from Kruijer et al., 2017).*

Other studies

Callahan et al. (2013) measured significant amounts of amino acids in RBT 04262 (Figure 22), higher than some carbonaceous chondrites, and argued that the extraterrestrial origin and nature of these should be further pursued.

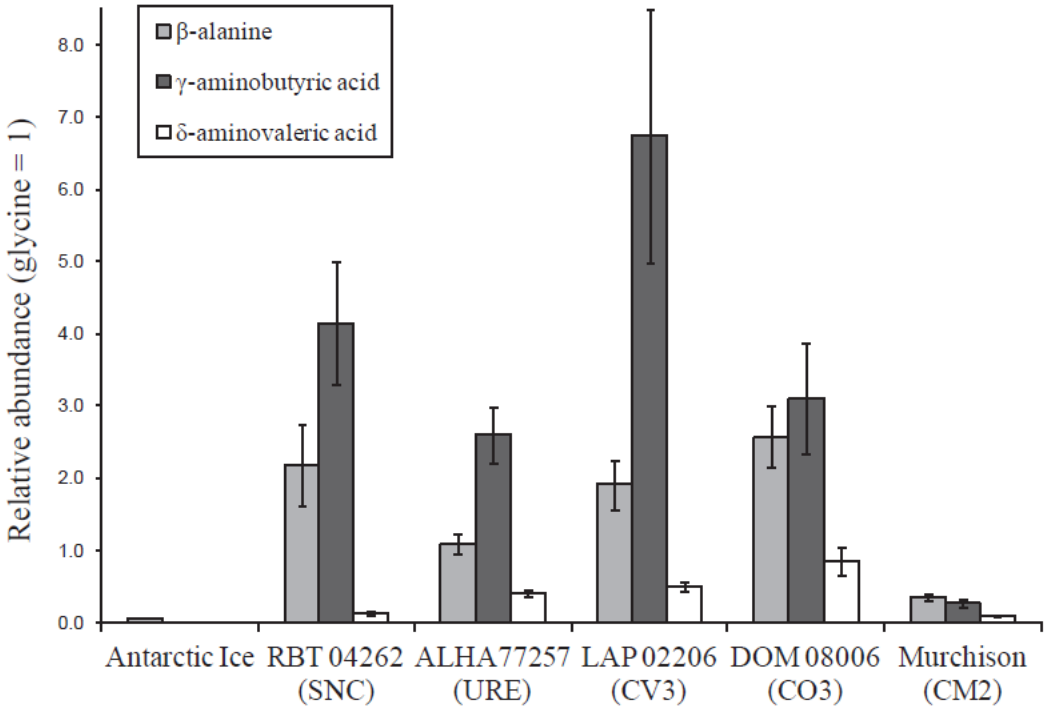

Figure 22: *Comparison of amino acids in RBT 04262 with those measured in ureilites and carbonaceous chondrites (from Callahan et al., 2013).*

Processing:

Processing details of RBT 04261 and RBT 04262 are presented here; a summary of how the samples have been subdivided, including potted butts and thin/thick sections, chips, and remaining usable mass, is presented in Figures 23 and 25. Both samples were initially subdivided into splits ,0, ,1, and ,4 or ,5 to prepare thin sections (,2) from a potted butt (,1) and have a chip on reserve in case oxygen isotopic analysis is required (Figures 23 to 26). After classification and announcement in the newsletter, the meteorites were further subdivided to fill sample requests. Images of typical subsplits of RBT 04261 and RBT 04262 are presented in Figures 24 and 26). For RBT 04261, 76.8% of original mass (mass of 0+5+13+14+15+48=60.5 g), and 18 thin/thick sections remain for future studies, while for RBT 04262, 74.2% of original mass (mass of 0+4+11+16+17+18+57+66+97-99=151.883 g), and 22 thick/thin sections remain for future studies. Figure 27 illustrates how one ~2 g chip of RBT 04262 was used to produce 8 thin sections.

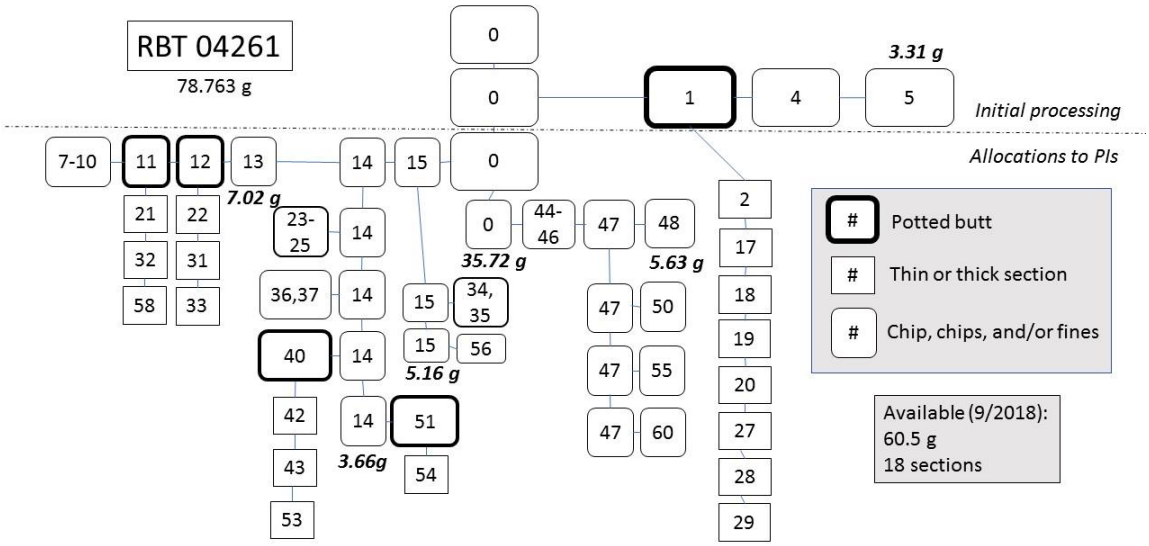

Figure 23: *Chart showing a summary of the subdivision of RBT 04261, including initial processing and later subdivision for allocations to PIs. Remaining 60.5 g of material represents 76.8% of original mass.*

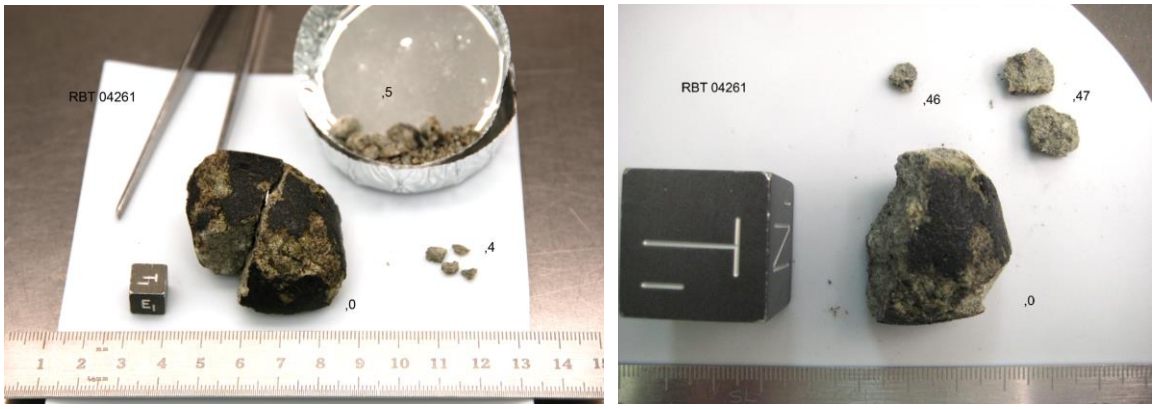

Figure 24: *Typical processing photos for RBT 04261, showing initial processing of the main mas into splits 0, 4, and 5 (left) and later subdivision of ,0 into ,46 and ,47 (right).*

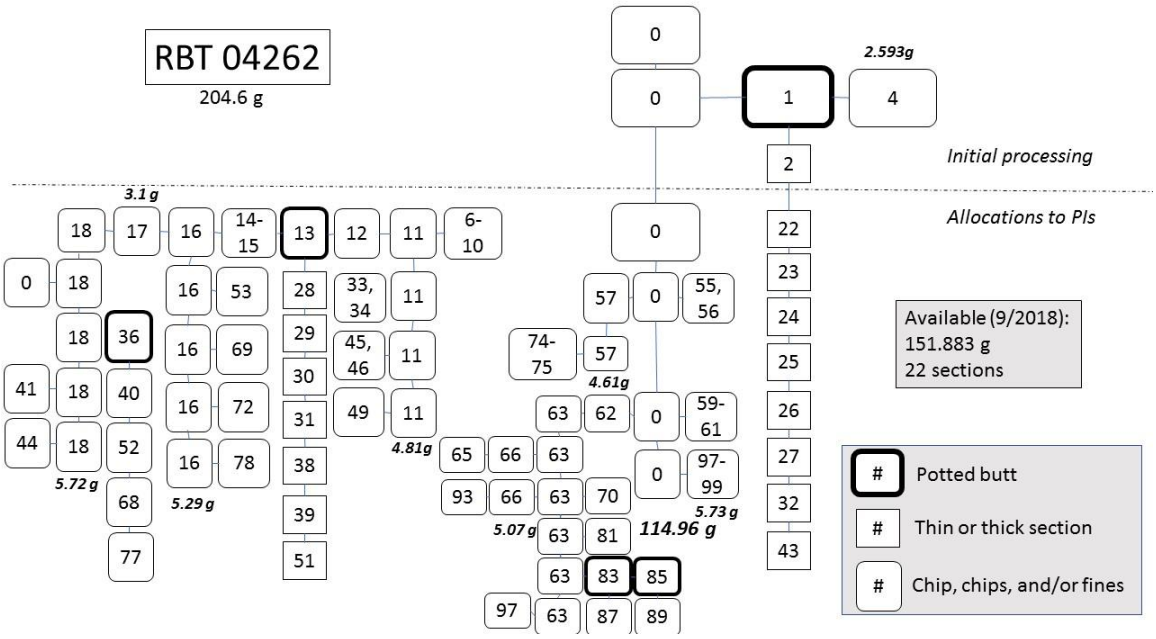

Figure 25: *Chart showing a summary of the subdivision of RBT 04262, including initial processing and later subdivision for allocations to PIs. Remaining 151.883 g of material represents 74.2 % of original mass.*

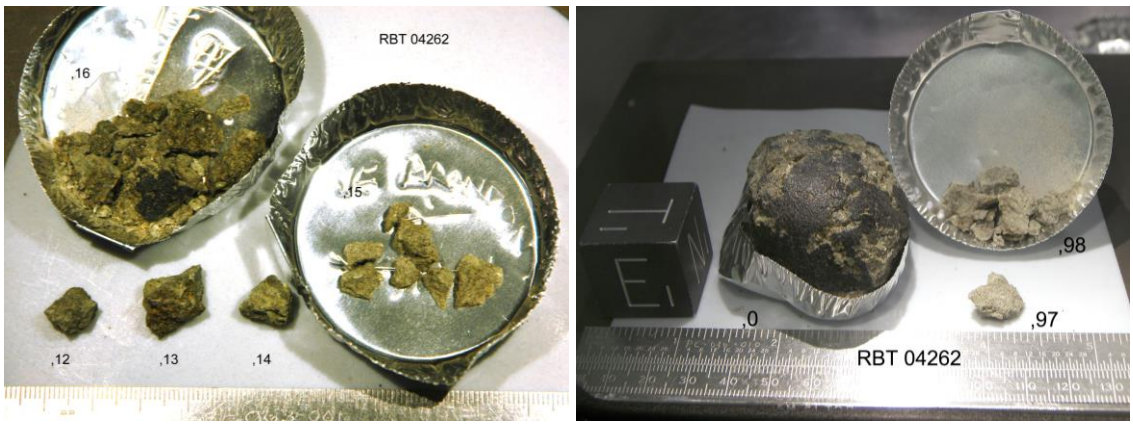

Figure 26: *Typical processing photos for RBT 04262, showing processing of split 16 into splits 12 to 15(left) and later subdivision of ,0 into ,97 and ,98 (right).*

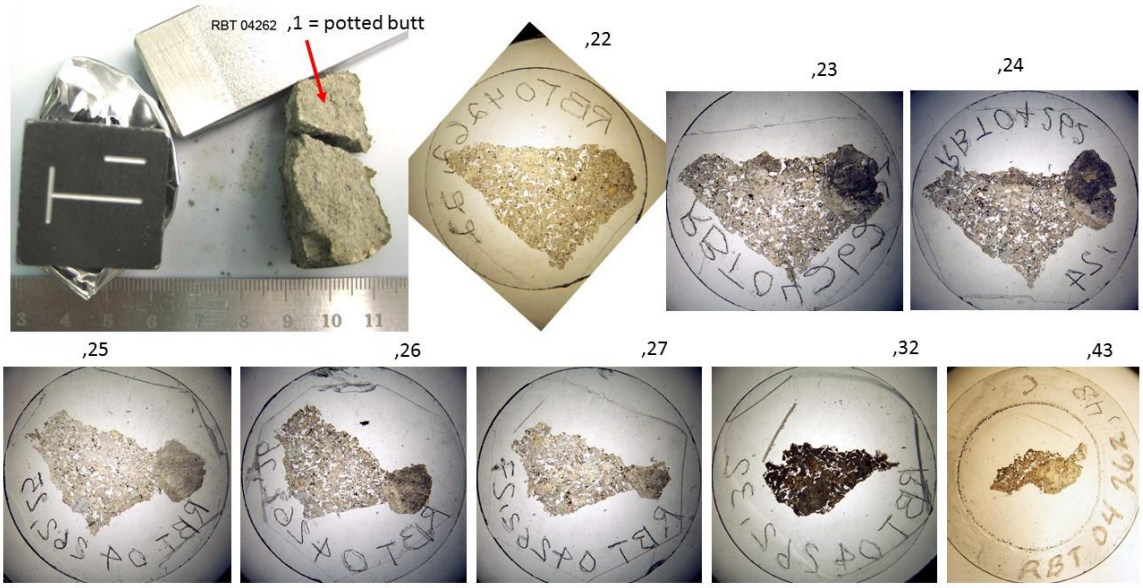

Figure 27: *RBT 04262 ,1 chip was used as a potted butt to make 8 thin sections that were provided for various scientific requests.*

References for RBT 04261 and RBT 04262

(originally compiled by C. Meyer, Oct. 2012 and updated by K. Righter Oct. 2018)

Bellucci, J. J., Nemchin, A. A., Whitehouse, M. J., Snape, J. F., Bland, P., Benedix, G. K., & Roszjar, J. (2018) Pb evolution in the Martian mantle. *Earth and Planetary Science Letters 485*, 79-87.

Bellucci, J. J., Whitehouse, M. J., John, T., Nemchin, A. A., Snape, J. F., Bland, P. A., & Benedix, G.K. (2017) Halogen and Cl isotopic systematics in Martian phosphates: Implications for the Cl cycle and surface halogen reservoirs on Mars. Earth and Planetary Science Letters 458, 192-202, https://doi.org/10.1016/j.epsl.2016.10.028.

Kruijer, T. S., Kleine, T., Borg, L. E., Brennecka, G. A., Irving, A. J., Bischoff, A., & Agee, C. B. (2017) The early differentiation of Mars inferred from Hf-W chronometry. Earth and Planetary Science Letters 474, 345-354, http://dx.doi.org/10.1016/j.epsl.2017.06.047.

Magna, T., Hu, Y., Teng, F. Z., & Mezger, K. (2017) Magnesium isotope systematics in Martian meteorites. Earth and Planetary Science Letters 474, 419-426, http://dx.doi.org/10.1016/j.epsl.2017.07.012.

Wang, Z., & Becker, H. (2017) Chalcophile elements in Martian meteorites indicate low sulfur content in the Martian interior and a volatile element-depleted late veneer. Earth and Planetary Science Letters 463, 56-68, http://dx.doi.org/10.1016/j.epsl.2017.01.023.

Wang, Z., & Becker, H. (2017) Silver contents and Cu/Ag ratios in Martian meteorites and the implications for planetary differentiation. Geochimica et Cosmochimica Acta 216, 96-114, http://dx.doi.org/10.1016/j.gca.2017.05.024.

Filiberto, J., Gross, J., McCubbin, F. M. (2016) Constraints on the water, chlorine, and fluorine content of the Martian mantle. Meteorit Planet Sci, 51, 2023-2035, doi:10.1111/maps.12624.

McCubbin, F. M., Boyce, J. W., Srinivasan, P., Santos, A. R., Elardo, S. M., Filiberto, J., Steele, A., Shearer, C. K. (2016) Heterogeneous distribution of H2O in the Martian interior: Implications for the abundance of H2O in depleted and enriched mantle sources. Meteorit Planet Sci 51, 2036-2060, doi:10.1111/maps.12639.

Williams, J. T., Shearer, C. K., Sharp, Z. D., Burger, P. V., McCubbin, F. M., Santos, A. R., Agee, C. B., McKeegan, K. D. (2016) The chlorine isotopic composition of Martian meteorites 1: Chlorine isotope composition of Martian mantle and crustal reservoirs and their interactions. Meteorit Planet Sci 51, 2092-2110, doi:10.1111/maps.12647.

Sharp, Z., Williams, J., Shearer, C., Agee, C., McKeegan, K. (2016) The chlorine isotope composition of Martian meteorites 2. Implications for the early solar system and the formation of Mars, Meteorit Planet Sci 51, 2111-2126, doi:10.1111/maps.12591.

Sossi, P.A., Nebel, O., Anand, M., Poitrasson, F. (2016) On the iron isotope composition of Mars and volatile depletion in the terrestrial planets, Earth and Planetary Science Letters 449, 360-371, ISSN 0012-821X.

Bloch, E., Ganguly, J. (2014) ^{176}Lu-^{176}Hf and ^{147}Sm-^{143}Nd ages of the Martian shergottites: Evaluation of the shock-resetting hypothesis through diffusion kinetic experiments and modeling, and petrological observations. Earth and Planetary Science Letters 395, 173-183.

Franz, H. B., Dottin Iii, J., Kim, S. T., Farquhar, J., Day, J. M. D., Economos, R. C., McKeegan, K. D., Schmitt, A. K., Irving, A. J., Hoek, J. (2014) Isotopic links between atmospheric chemistry and the deep sulphur cycle on Mars. Nature 508, 364-368.

Schwenzer, S. P., Hammond, S., Franchi, I. A., Greenwood, R. C., Kelley, S. P., Ott, U., Tindle, A. G., Haubold, R., Herrmann, S., Gibson, J. M., Anand, M. (2013) Quantifying noble gas contamination during terrestrial alteration in Martian meteorites from Antarctica. Meteoritics & Planetary Science 48, 929-954, http://dx.doi.org/10.1111/maps.12110.

Callahan, M. P., Burton, A. S., Elsila, J. E., Baker, E. M., Smith, K. E., Glavin, D. P., Dworkin, J. P. (2013) A search for amino acids and nucleobases in the Martian meteorite Roberts Massif 04262 using liquid chromatography-mass spectrometry. Meteoritics & Planetary Science 48, 786-795, http://dx.doi.org/10.1111/maps.12103.

Brandon, A. D., Puchtel, I. S., Walker, R. J., Day, J. M. D., Irving, A. J., Taylor, L. A. (2012) Evolution of the Martian mantle inferred from the ^{187}Re-^{187}Os isotope and highly siderophile element abundance systematics of shergottite meteorites, Geochimica et Cosmochimica Acta 76, 206-235, http://dx.doi.org/10.1016/j.gca.2011.09.047.

Niihara, T. (2011) Uranium-lead age of baddeleyite in shergottite Roberts Massif 04261: Implications for magmatic activity on Mars. Journal of Geophysical Research: Planets 116(E12), (1991-2012).

Usui, T., Sanborn, M., Wadhwa, M., Mcsween Jr., H. Y (2010) Petrology and trace element geochemistry of Robert Massif 04261 and 04262 meteorites, the first examples of geochemically enriched lherzolitic shergottites, Geochimica et Cosmochimica Acta 74, 7283-7306, http://dx.doi.org/10.1016/j.gca.2010.09.010.

Cartwright, J. A., Ocker, K. D., Crowther, S. A., Burgess, R., Gilmour, J. D. (2010) Terrestrial and Martian weathering signatures of xenon components in shergottite mineral

separates. Meteoritics & Planetary Science 45, 1359-1379, http://dx.doi.org/10.1111/j.1945-5100.2010.01101.x.

Bouvier, A., Blichert-Toft, J., Albarede, F. (2009) Martian meteorite chronology and the evolution of the interior of Mars, Earth and Planetary Science Letters 280, 285-295, http://dx.doi.org/10.1016/j.epsl.2009.01.042.

Papike, J. J., Karner, J. M., Shearer, C. K., Burger, P. V. (2009) Silicate mineralogy of martian meteorites, Geochimica et Cosmochimica Acta 73, 7443-7485, http://dx.doi.org/10.1016/j.gca.2009.09.008.

Shearer, C. K., Burger, P. V., Papike, J. J., Borg, L. E., Irving, A. J., Herd, C., (2008) Petrogenetic linkages among Martian basalts: Implications based on trace element chemistry of olivine. Meteoritics & Planetary Science 43, 1241-1258, http://dx.doi.org/10.1111/j.1945-5100.2008.tb01126.x.

Anand M., James S., Greenwood R.C., Johnson D., Franchi I.A. and Grady M.M. (2008) Mineralogy and geochemistry of Shergottite RBT04262 (abs#2173). *Lunar Planet. Sci*. XXXIX Lunar Planetary Institute, Houston.

Beckett J.R., McCanta M.C. and Stolper E.M. (2008) Phosphorus zoning in SNC olivines (abs#1726). *Lunar Planet. Sci*. XXXIX. Lunar Planetary Institute, Houston.

Brandon A.D., Puchtel I.S., Walker R.J., Day J.M.D., Irving A.J. and Taylor L.A. (2012) Evolution of the Martian mantle inferred from the ^{187}Re-^{187}Os isotope and high siderophile element systematics of the Shergottite meteorites. *Geochim. Cosmochim. Acta* 76, 206-235.

Cartwright J.A., Burgess R., Crowther S.A. and Gilmour J.D. (2008) Xenon isotope composition of Shergottite RBT 04262 (abs#2000). *Lunar Planet. Sci*. XXXIX. Lunar Planetary Institute, Houston.

Cartwright J.A., Burgess R. and Gilmour J.D. (2009a) Xenon isotopes in Shergottites RBT 04262, DAG 489, Shergotty and EET 79001 (abs#1907). *Lunar Planet. Sci.* XL, Lunar Planetary Institute @ The Woodlands.

Cartwright J.A., Burgess R. and Gilmour J.D (2009b) Halogens in Martian Shergottite RBT 04262 (abs#1686). *Lunar Planet. Sci.* XL, Lunar Planetary Institute @ The Woodlands.

Cartwright J.A., Ocker K.D., Crowther S.A., Burgess R. and Gilmour J.D (2009c) Terrestrial and Martian weathering signatures of Xenon components in Shergottite mineral separates. *Meteorit. & Planet. Sci*. 45, 1359-1378.

Cartwright J.A. and Burgess R. (2011) Ar-Ar crystallization ages of Shergottite RBT04262 mineral separates (abs#5465). *Meteorit. & Planet.*46, A36.

Connolly H.C. and 7 authors (2007b) The Meteoritical Bulletin, No. 92, 2007 September. *Meteorit. & Planet. Sci.* 42, 1647-1694.

Greenwood, J. P., Itoh, S., Sakamoto, N., & Yurimoto, H. (2009) Hydrogen Isotope Measurements of Gypsum and Jarosite in Martian Meteorite Roberts Massif 04262: Antarctic and Houstonian Weathering. In 40th *Lunar and Planetary Science Conference*, #2528.

Dalton H.A., Peslier A.H., Brandon A.D., Lee C-T.A. and Lapen T.J. (2008) Petrology and mineral chemistry of new olivine-phyric Shergottite RBT04262 (abs#2308). *Lunar Planet. Sci*. XXXIX. Lunar Planetary Institute, Houston.

Franz H.B., Farquhar J. and Kim S.T. (2008) Sulfur isotopic composition of multiple mineral phases in Shergottites (abs#2433). *Lunar Planet. Sci*. XXXIX. Lunar Planetary Institute, Houston.

Karner J.M., Harvey R.P. and Alpert S. (2010) Are Martian meteorites RBT 04261 and RBT 04262 really paired? A petrologic and geochemical study (abs#5354). *Meteorit. & Planet. Sci.* 45, A100.

Lapen T.J., Brandon A.D., Beard B.L., Peslier A.H., Lee C-T.A. and Dalton H.A. (2008) Lu-Hf age and isotopic systematics of the olivine-phyric Shergottite RBT-04262 and implications for the source of enriched Shergottites (abs#2073). *Lunar Planet. Sci*. XXXIX. Lunar Planetary Institute, Houston.

Mikouchi T. (2008) Petrographic and chemical variation of Lherzolitic Shergottites and implications for the classification of Shergottites (abs) *Meteorit. & Planet. Sci.* 43, A186.

Mikouchi T., Kurihara T. and Miyamoto M. (2008) Petrology and mineralogy of RBT04262: Implications for stratigraphy of the Lherzolitic Shergottite igneous block (abs#2403). *Lunar Planet. Sci*. XXXIX. Lunar Planetary Institute, Houston.

Mittlefehldt D.W. and Herrin J.S. (2008) Petrology and geochemistry of Martian meteorites LAR06319, RBT 04261 and RBT 04262 (abs#5307). *Meteorit. & Planet. Sci.* 43, A100.

Nagao K. and Park J. (2008) Nobel gases and cosmic-ray exposure ages of two Martian Shergottites, RBT 04262 and LAR 06319 recovered in Antarctica (abs#5200). *Meteorit. & Planet. Sci.* 43, A107.

Niihara T. (2011) Uranium-lead age of baddeleyite in Shergottite Roberts Massif 04261: Implications for magmatic activity on Mars. *J. Geophys. Res.*116, *E12008, doi: 10.1029/2011JE003802*

Niihara T. (2012) Correction to "Uranium-lead age of baddeleyite in Shergottite Roberts Massif 04261: Implications for magmatic activity on Mars. *J. Geophys. Res.*117, *E02002, doi:10.1029/2012JE004048*

Niihara T., Misawa K. and Kaiden H. (2010) Young U-Pb age of baddeleyite in enriched Shergottite RBT 04261 (abs#5207). *Meteorit. & Planet. Sci.* 45, A152.

Nishiizumi K. and Caffee M.W. (2010) A tale of two Shergottites: RBT04261 and RBT04262 (abs#2276). *Lunar Planet. Sci.* XLI Lunar Planetary Institute, Houston. (*Houston, we have a problem)*

Papike J.J., Karner J.M., Spilde M.N., Shearer C.K. and Burger P.V. (2009b) Silicate mineralogy of Martian meteorites. *Geochim. Cosmochim. Acta* 73, 7443-7485. *(invited review with great pictures of textures)*

Satake W., Mikouchi T. and Miyamoto M. (2009a) Redox state of geochemically-enriched "Lherzolitic" Shergottites as inferred from Fe Micro-XANES analysis (abs). *Antarctic Meteorites* XXXII 64-65.

Shearer C.K., Burger P.V., Papike J.J., Borg L.E., Irving A.J. and Herd C. (2008) Petrogenic linkages among Martian basalts: Implications based on trace element chemistry of olivine. *Meteorit. & Planet. Sci*. 43, 1241-1258.

Shearer C.K., Burger P.V., Papike J.J. and Karner J. (2009) Comparison between RBT04262 and Lherzolitic Shergottites (ALHA77005 and LEW88516) (abs#1300). *Lunar Planet. Sci.* XL, Lunar Planetary Institute, The Woodlands.

Shih C-Y., Nyquist L.A. and Reese Y. (2009a) Rb-Sr and Sm-Nd studies of olivine-pyric Shergotties RBT04262 and LAR06319: Isotopic evidence for relationship to enriched basaltic Shergottites (abs#1360). *Lunar Planet. Sci.* XL, Lunar Planetary Institute @The Woodlands.

Usui T., Sanborn M.E., Wadhwa M. and McSween H.Y. (2008a) Petrogenesis of geochemically enriched Lherzolitic Shergottites RBT04261 and RBT04262 (abs#5052). *Meteorit. & Planet. Sci.* 43, A159.

Usui T., Sanborn M.E., Wadhwa M. and McSween H.Y. (2010) Petrology and trace element geochemistry of Robert Massif 04261 and 04262 meteorites, the first examples of geochemically enriched Lherzolitic Shergottites. *Geochim. Cosmochim. Acta* 74, 7283-7306.

Walker R.J., Putchel I.S., Brandon A.D., Day J.M.D. and Irving A.J. (2009) Re-Os and highly siderophile element systematics of Shergottites: New puzzles regarding the Martian mantle (abs#1263). *Lunar Planet. Sci.* XL, Lunar Planetary Institute, @ The Woodlands.

K. Righter, October 2018